

THE STATUS OF THE NEW HIGH-DYNAMIC DCM FOR SIRIUS

R. R. Geraldes^{†1}, R. M. Caliarì, G. B. Z. L. Moreno, M. Saveri Silva, L. Sanfelici,
H.C.N. Tolentino, H. Westfahl Jr., Brazilian Synchrotron Light Laboratory (LNLS),
Brazilian Center for Research in Energy and Materials (CNPEM), Campinas, São Paulo, Brazil
T. A. M. Ruijl, R. M. Schneider, MI Partners, Eindhoven, The Netherlands
¹also at Technische Universiteit Eindhoven, Eindhoven, The Netherlands

Abstract

The monochromator is known to be one of the most critical optical elements of a synchrotron beamline, since it directly affects the beam quality with respect to energy and position. Naturally, the new 4th generation machines, with their small emittances, start to bring higher stability performance requirements, in spite of factors as high power loads and variations, high radiation levels, ultra-high vacuum compatibility and vibration sources. In response to that, an innovative concept of a high-dynamic vertical DCM (Double Crystal Monochromator) with angular range between 3 and 60 degrees (equivalent to 2.3 to 38 keV with Si(111)) has been developed at the Brazilian Synchrotron Light Laboratory. A highly repeatable dynamic system, with servo control bandwidth of 250 Hz, has been achieved and will be installed at Sirius macromolecular crystallography beamline – MANACA – still in 2018. The complete offline results of the in-vacuum cryocooled high-dynamic DCM, showing stability between crystals around 15 nrad RMS up to 2.5 kHz, even during the Bragg angle motion for flyscans, are presented.

INTRODUCTION

The beamlines of the new generation of synchrotrons, the so-called Diffraction Limit Storage Rings (DLSR), have started to be built with ever more demanding requirements to preserve the extraordinary properties of the sources. In double-crystal monochromators (DCMs), the main performance bottleneck has been proven to be the stability of the parallelism between the two crystals, since it affects the position of the virtual source with a scaling factor given by the distance to the source, which is typically about 30 m [1]. Indeed, for sources of a few microns, this angular stability must be kept within a few nrad to keep the variation of the virtual source within about 10% of its size.

Considering the frequency range between 0 and 2.5 kHz, figures as low as 20 nrad RMS (root mean square) have been reported for horizontal DCMs [2], whereas for vertical DCMs the best performances seemed to be stuck around 50 nrad RMS [3]. Yet, it must be noticed that still today most of the available data about DCMs unfortunately cannot be directly compared to each other. This is because, although for given disturbance levels the outcome of a measurement does strongly depend on acquisition parameters like frequency and integration time, the RMS values are hardly ever displayed as a function of frequen-

cy, but often mentioned as single numbers without further acquisition details. This means that many official numbers show averaged optimistic values, which may not be consistent with the needs and timescales of different experiments at the beamlines. Indeed, with experiments reaching the sub-millisecond range, performances in the kHz range must be proven. Moreover, it must be emphasized that even the best results rely on braked systems only, whereas about 100 nrad RMS could be expected in active control [3]. Finally, during energy flyscans, the stability levels may exceed the microradian range. Consequently, to the best of our knowledge, no vertical DCM had been close to the 10-nrad-level performance as required by DLSR beamlines.

Convinced that incremental improvements in traditional systems was insufficient to reach the new requirements, the Brazilian Synchrotron has developed over the last three years an innovative DCM, the so-called High-Dynamic DCM (HD-DCM), an active high-performance mechatronic system with a closed-loop bandwidth of 250 Hz [4]. The conceptual design, the mechatronic principles and thermal management solutions were presented in MEDSI 2016 [5–7]. More recently, the results of in-air validation of the core, together with system identification and control techniques, were presented in ICALEPCS 2017 [8,9]. In the following sections, the most recent updates, together with the offline performance of the full in-vacuum cryocooled system, are presented, showing unprecedented stability and scanning performances.

The HD-DCM is now ready to be tested online and is expected to be installed at Sirius macromolecular crystallography beamline – MANACA – in the second semester of 2018. Sirius is in an advanced construction phase, with the LINAC and the booster currently being commissioned and installed, respectively.

SYSTEM STATUS

Goniometric System

Figure 1 shows the complete system and highlights its sub-modules, including the goniometric system, the vacuum vessel and the granite bench, which were not addressed in previous publications.

As planned from the beginning, the goniometric system was realized by means of double-side bearings, to improve the load capacity and stiffness in a symmetric design. To save development time and costs, a commercial direct-drive ball-bearing rotary stage has

[†] renan.geraldes@lnls.br

Content from this work may be used under the terms of the CC BY 3.0 licence (© 2018). Any distribution of this work must maintain attribution to the author(s), title of the work, publisher, and DOI.

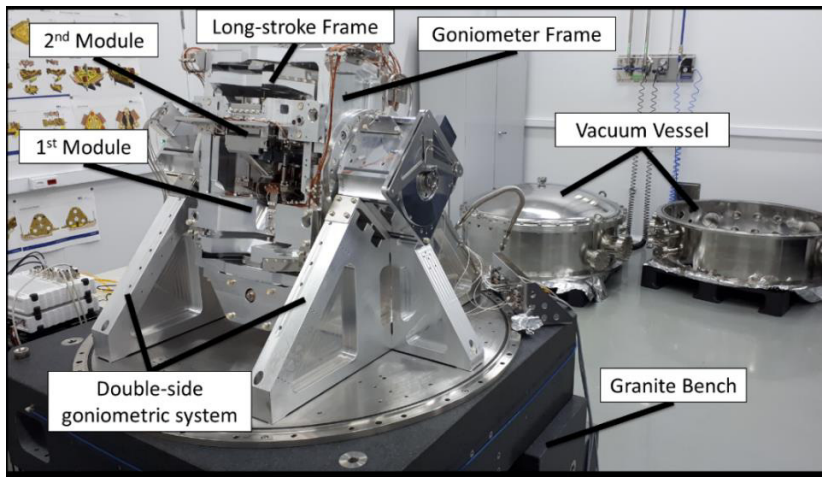


Figure 1: Overall view of the HD-DCM with its major subparts, namely: granite bench, double-side goniometric system, goniometer frame, long-stroke frame, 1st and 2nd modules, and the vacuum vessel. (For references, see [5].)

been selected, being enough to have one active stage and an equivalent passive bearing at the opposite side. The supports consist of aluminium frames, designed for maximum supporting stiffness while preventing excessive loads and deformations in the bearings, which might lead to loss of performance and premature wear. Before assembling the core, the rotary stages were mounted to the supports and aligned to each other with a laser tracker within 250 μm and 0.6 mrad. The residual misalignment is within the design budget of the elastic membranes that couple the stages to the goniometer frame.

The supports are deterministically mounted to the bottom flange of the vacuum vessel, which, in turn, is clamped to the top element of the granite bench, both from the top side in the perimeter and from below in the center. This way, the internal mechanics may greatly benefit from the stiffness of the granite bench. The vessel is completed by a bottom section, with all functional feed-throughs, a top section, with viewports and beam entrance and exit ports, and a cover. Sealing between these parts can be made either with o-rings or elastic seals. The granite bench is a topic in its own and more details are given in [10].

For the moment a closed-loop control bandwidth of 25 Hz has been used to control the Bragg angle with in-position stability of 24 nrad RMS up to 2.5 kHz. It is worth mentioning that, although this measurement is indirectly given by the encoder inside the rotary stage, not only does the core have a large moment of inertia (12 kg.m²), but also the rotor of the stages decouples from it at about 1.2 kHz, so that the real stability with respect to the bench is expected to be very close to this value. This does not take the tilting of the bench with respect to the floor into account, but this shall be evaluated by other means at the beamline.

Crystal Alignment

The Si(111) and Si(311) crystals have been designed for high eigenfrequencies and deterministic performance with respect to their metrology frames, while allowing for

cooling and beam propagation compatibilities. Both crystal sets, with their unusual triangular shapes and extended ears to increase rotational modes, have been manufactured by the team of Elina Kasman at the Advanced Photon Source (APS). Figure 2 shows the crystals during inspection in a coordinate measurement machine (CMM).

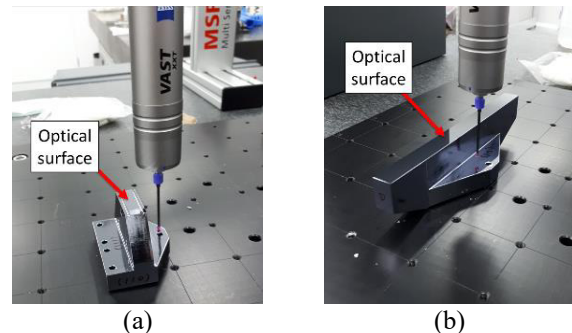


Figure 2: 1st and 2nd crystals being inspected at CMM.

Crystallographic orientation and machining tolerances are inherent limitations in the manufacturing process of crystals, such that in these crystals the angles between the diffraction planes and the bottom surface of the crystals, which make the interface with the metrology frames, reached as much as 0.17°. Therefore, as the interferometers used in the embedded metrology loop have angular operational range around $\pm 0.1^\circ$, an alignment procedure has been developed to bring the parallelism between the diffraction planes and surfaces of the mounting surfaces down to the millidegree range by means of dedicated machined shims. The procedure is based on an iterative process of measurements made in the diffractometer of the XRD2 beamline at LNL and at a CMM, as seen in Fig. 3, and fine machining of the shims. The results after two iterations are shown in Table 1, where the values were systematically reduced to at least 0.002°, which is the estimated practical repeatability limitation of the overall process. The value for the 2nd crystal of Si(111) in roll was intentionally made relatively larger to test practical aspects of the technique, but it does not affect the tuning between crystals.

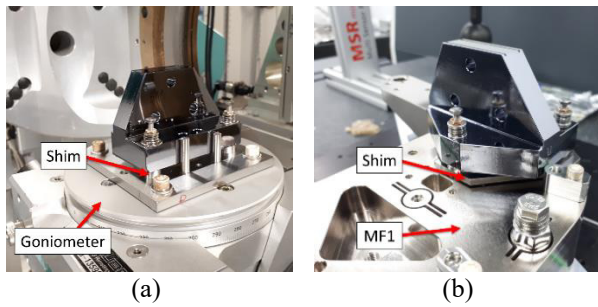


Figure 3: Parallelism correction procedure: (a) crystal on diffractometer at XRD2 beamline at LNLS; (b) crystal on metrology frame (MF1) during measurements at a CMM.

Table 1: Parallelism

	Pitch [deg]		Roll [deg]	
	before	after	before	after
1 st Si(111)	0.054	0.002	0.087	0.005
1 st Si(311)	0.173	0.003	0.043	0.002
2 nd Si(111)	0.026	0.002	0.131	0.012
2 nd Si(311)	0.015	<0.001	0.172	0.003

Manifold

The stainless-steel manifold that had been designed for reducing flow-induced vibrations in the system [11] was produced by additive manufacturing (3D-printing) by the team of Prof. Andre Jardini from the University of Campinas (UNICAMP). Next, to improve external surface roughness for vacuum purposes and refine the more precise dimensions, it went through a finishing machining step at LNLS' workshop. Finally, the full assembly, with the previously brazed tripartite copper cooling blocks and the stainless-steel tubes, was brazed by the Materials group at LNLS. Related pictures are shown in Fig. 4.

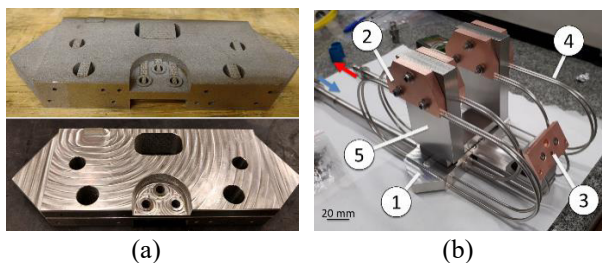


Figure 4: (a) 3D-printed manifold as sintered (top) and after finishing machining. (b) Assembly mounted to brazing tooling: manifold (1), cooling block (2) (x4), manifold extension (3), distribution tubes (4) (x18), and tooling (5).

Furthermore, to effectively compare the influence of the optimized flow distribution in the performance of the HD-DCM with that of a non-optimized design, another assembly was manufactured with a manifold produced by simple machining and welding processes. Indeed, as shown in the Results section, both have been tested in operational conditions with significant differences in the final stability levels. Figure 5 shows an isometric section view of the two manifold designs, with the optimized solution, resembling arteries, in (a), and a simple design, with abrupt flow changes in (b).

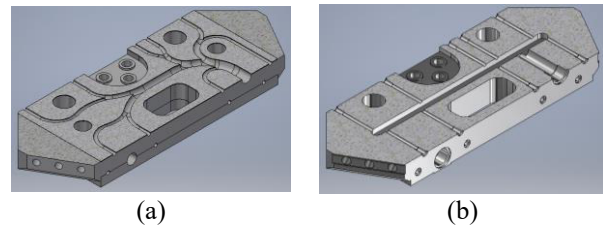


Figure 5: Isometric section view of two manifold designs: (a) optimized solution, resembling arteries; (b) simple design, with abrupt flow changes.

Thermal Management

The system includes 20 RTDs (resistance temperature detector) divided in two types, namely: PT10K, for low-temperature measurements, and PT2K, for room-temperature measurements. Some are used for monitoring purposes only, whereas the others are used in active temperature control of a few critical parts. Particularly, the Y-frame (YFM) and the short-stroke frame (SHF) are parts with direct interface with the crystal modules. So, to control heat leakage and avoid cooling of adjacent parts, they are actively temperature controlled at 24°C by local heaters in closed-loop. The temperature of the 2nd crystals are controlled at 155 K to match the lattice parameter of the 1st crystals. Finally, some heating power is put on the voice coils (VCF) to stabilize their temperature regardless the operation condition of the HD-DCM. This control is achieved by means of 16 low-power (up to 4 W) Kapton foil heaters.

Except for the actual beam power load, all the remaining thermal aspects have been evaluated offline. Table 2 compares the designed with the final temperature distribution of the parts, showing that the desired temperatures of sensitive elements have been successfully met. The main differences were found in the SHS and the VCFs, due to blackbody radiation absorption over limited thermal conductivity links.

Table 2: Comparison between Designed and Experimental Offline Temperature Distribution. (For element reference, see [5].)

Element	Designed [K]	Experimental [K]
CR1	78	78
MF1	170	180
YFM	297	297
BRC	95	102
CR2	155	155
SHS	210	250
VCF	250	267
SSF	297	297

Except for the first crystals, which reach the operational temperature in just a few minutes due to the very efficient cooling scheme, the time constants of the remaining parts are relatively large. The consequence is two-fold: on the one hand, the complete cooldown thermalization is in the order of 24 hours, which can be somewhat inconvenient; on the other hand, however, the system will probably be rather insensitive to fast power load variations, which

Content from this work may be used under the terms of the CC BY 3.0 licence (© 2018). Any distribution of this work must maintain attribution to the author(s), title of the work, publisher, and DOI.

may not only simplify the timing requirements in the temperature control loop, but also minimize thermal-drift problems in most scanning applications. Studies for more advanced thermal control strategies, including feedforward are currently in progress.

SYSTEM PERFORMANCE

In-position Performance

As mentioned, analysing the system as a function of frequency is of fundamental importance to understanding the different effects that the mechanical instabilities may have. Therefore, the cumulative amplitude spectrum (CAS) (in [SI]), which is the square root of the cumulative power spectrum (CPS) (in [SI²]) and provides the integrated RMS value as a function of frequency, has been chosen as the standard output format for performance evaluation.

Figure 6 shows the in-position relative pitch (*ShsRx*) performance of the HD-DCM up to 2.5 kHz as measured by the embedded interferometric metrology system for different LN₂ flows, both for the 3D-printed (solid lines) and the machined (dashed lines) manifold assemblies. It is clear from the data that all experimental conditions show virtually the same error levels up to about 300 Hz, with an RMS value close to 5 nrad. This is a direct result of the efficiency of the closed-loop control of the short-stroke module, with a bandwidth of 250 Hz. Also clear is the positive impact of the optimized manifold solution, typically reducing the integrated values up to 2.5 kHz by a factor 2. Indeed, the greatest contribution for the total errors (even more clearly seen in PSD spectra) is the internal resonance at about 450 Hz, namely, the first mode between the metrology frame of the 1st crystals and the YFM, which is directly excited by the flow disturbances in the manifold. Considering the optimized manifold, RMS_{2.5kHz} values are between 12 and 25 nrad. In terms of roll (*ShsRz*) and gap (*ShsY*) stabilities, similar results are found, with typical values of 18 nrad and 1.8 nm RMS_{2.5kHz}, respectively. All measurements were made over periods of 10 s.

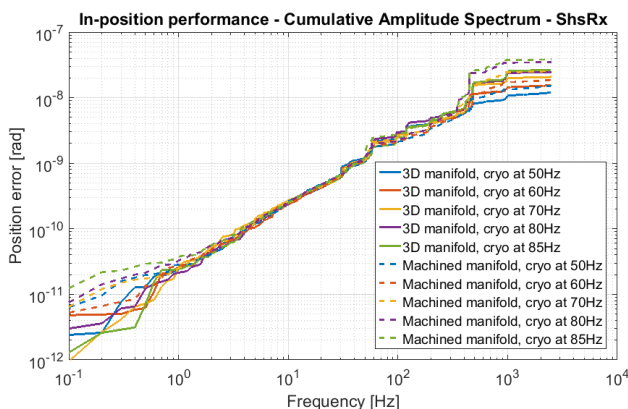


Figure 6: In-position CAS for the relative pitch between crystals (*ShsRx*), taken at different flow levels, both with the 3D-printed and the machined manifold assemblies.

The flowmeter of the cryocooler was not functioning, so, unfortunately, the only parameter available for comparisons was its pumping frequency. For reference, from preliminary measurements, 60 Hz and 85 Hz are estimated to reflect flows of 4 and 6 l/min, respectively. The actual operational flow will be determined online.

Two relevant comments need to be made regarding measurement noise levels and the indirect metrology. Evaluating the noise levels of the interferometers up to high frequencies require careful experimental investigations. Preliminary analyses suggest that in vacuum these levels would be at least below 0.5 nm, translated to and 5 nrad RMS_{2.5kHz}, which was considered good enough for the moment. Next, the interferometers do not directly see the relative position between the crystals, which can only be evaluated with enough resolution and bandwidth at the beamline. However, modal analyses realized in the 1st module suggest that the decoupling frequencies between the metrology frame and the crystals indeed exceed 1 kHz, as targeted in design. Then, the errors that are invisible to the interferometers are expected to have very small contribution.

Finally, it is worth mentioning that, the rotary stage is constantly under control, i.e. the results do not depend on additional brakes or limited operational conditions. Measurements made with brakes engaged to the rotary stage did not result in any improvement in performance.

Scanning Performances

Considering the dynamic concept of the HD-DCM, more interesting than the in-position performance is the scanning capacity of the instrument. Thanks to the two-level design, two energy scan modes are available:

Standard scanning mode In the standard mode, the Bragg angle is a setpoint to both the long-stroke and the short-stroke modules, which move together to adjust the gap while stabilizing pitch and roll. Thus, scans of any size can be made within the operational energy range. However, specially at low energies, for which large motions are required, the stability levels suffer from disturbances of the stepper-driven long-stroke actuator.

High-performance scanning mode In the alternative mode, the long-stroke is kept still while the Bragg setpoint is sent to the short-stroke only. Naturally, the scan ranges become limited to reasonable gap ranges in the short-stroke. However, particularly for energies above 8 or 10 keV, more than 1 keV scans can be performed with virtually the same stability levels of in-position performance even for scanning speeds as high as 1 keV/s.

Figure 7 shows *ShsRx* RMS_{2.5kHz} values for scans in standard and high-performance modes. As cases of interest, 1keV scans were made around different energy values for different speeds, so that every point in the graph corresponds to the CAS value at 2.5 kHz for a full scan with constant eV/s speed. In standard mode, at 20 and 30 keV the angular and gap motions are small, so that the performance is equivalent to in-position stability. As the energy

is reduced, however, the stroke and speed of the long-stroke actuator get increasingly larger, with clear disturbing effects, reaching as much as 80 nrad RMS_{2.5kHz} around 3 keV, for example. It is also worth noticing that around 3 and 5 keV the scanning speeds are limited to 30 eV/s and 100 eV/s, respectively. This is due to a practical limit of about 1 mm/s in the variation of the gap between the crystals, which is partly given by present speed limitations in the acquisition rate of the interferometers, but also by acceleration levels and heat dissipation limitations in the mechanics and actuators, respectively. Regarding the high-performance mode, 3 keV has very limited range and even 5 keV is limited to 500 eV scans. Above 10 keV, however, 1keV scans are perfectly feasible. Moreover, up to 1 keV/s all points overlap with performances around 15 to 18 nrad RMS_{2.5kHz}. Then, above 1 keV/s, high speeds and accelerations are present and the error levels increase. Nonetheless, significant improvement can be expected with feedforward control (not yet implemented).

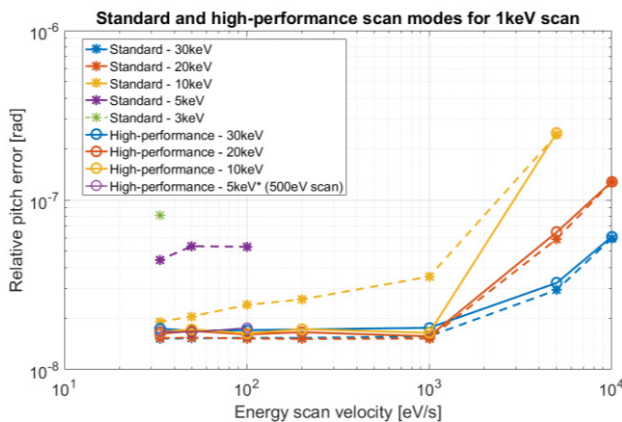


Figure 7: RMS_{2.5kHz} relative pitch between crystals (ShsRx) for standard and high-performance 1 keV scans for speeds between 30 and 10.000 eV/s.

Source Degradation Frequency Analysis

In the beginning of the project, the desired target for *ShsRx* was 10 nrad peak (3σ) up to 2.5 kHz. However, this is even probably limited by the noise floor of the interferometers alone. Yet, with the present results, 3σ 10 nrad is achieved somewhere between 100 and 200 Hz. Therefore, evaluating the effective source degradation effects as a function of frequency may be an instructive exercise. Figure 8 shows the equivalent RMS values of the maximum vertical position deviation of the virtual source and its size increase in microns for a 30-meter distance between source and monochromator as a function of the integration time for a typical stability CAS. For integration times above 100 ms all instabilities are reflected as an increase in source size. For a source of 10 μ m FWHM, the size increase is of about 2.5%, if quadratic sum is used. At the other extreme, for integration times in the order of 1 ms, most of the instabilities are reflected as position deviations of the source, with minimum effect in size increase. Again considering a source of 10 μ m FWHM, the RMS deviation is about 9.5% of the size, which is still within the initial specifications.

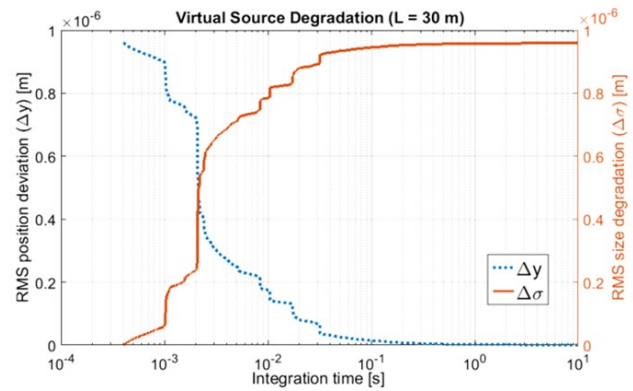


Figure 8: RMS values for virtual source vertical size degradation and maximum position deviation as a function of integration time for typical *ShsRx* instability levels (16 nrad RMS_{2.5kHz}) in the HD-DCM for a distance of 30 m.

CONCLUSIONS

The offline characterization of the HD-DCM proved cryogenic operation and showed performance around 15 nrad RMS_{2.5kHz} for in-position pitch stability. More remarkably, it was shown that even 1keV energy scans at up to 1 keV/s can be made with the same performance. Intrinsic limitations of an embedded metrology system, as insensitiveness to deviations associated to cosine, cyclic and Abbe errors, or thermal and wavelength instabilities, for instance, can be in principle greatly reduced via calibration, thanks to the high repeatability that is obtained by the design principles upon which the system is based. Finally, the high eigenfrequencies in the metrology loop reduces the dynamic errors in the indirect metrology to a minor contribution. In any case, the achieved results must naturally be validated under operational conditions at the beamline.

FUTURE WORK

The control platform is currently being migrated from Speedgoat's xPC to National Instruments' cRio. Moreover, in the near future, feedforward and optimized thermal control are expected to be implemented soon. The unit that is ready is expected to be installed at the MANACA beamline in the second semester of 2018 to start online commissioning. A second unit is in production and should be installed shortly after at the EMA beamline. Finally, an upgrade in the LOS actuator has been designed, with the purpose of allowing for high-performance scanning over the full energy range.

ACKNOWLEDGEMENTS

The authors would like to gratefully acknowledge the funding by the Brazilian Ministry of Science, Technology, Innovation and Communication, the contributions of the LNSL team, the MI-Partners team and those of the synchrotron community who directly or indirectly built the path to this development, and also the collaboration with Elina Kasman's team at APS.

REFERENCES

- [1] *ESRF DCM Workshop*, Grenoble, France, May 2014, unpublished.
- [2] P. Kristiansen, “Vibrational Stability of a Cryocooled Horizontal-Bounce Double Crystal Monochromator”, presented at MEDSI’16, Barcelona, Spain, Sept. 2016, paper TU-CA04, unpublished.
- [3] P. Kristiansen, J. Horbach, R. Doehrmann, J. Heuer *et al.*, “Vibration measurements of high-heat-load monochromators for DESY PETRA III extension”, *J. Synchrotron Rad.*, vol. 22, pp. 879-885, Jul. 2015.
- [4] R. R. Geraldes *et al.*, “Instrumento para movimentação de posicionamento de elementos ópticos com resolução e estabilidade mecânica nanométricas em linhas de luz”, PCT/BR2017/050262, 2017, Patent Pending.
- [5] R. R. Geraldes *et al.*, “The New High Dynamics DCM for Sirius”, in *Proc. MEDSI’16*, Barcelona, Spain, Sep. 2016, paper TUCA05, pp. 141-146, doi : 10.18429/JACoW-MEDSI2016-TUCA05
- [6] R. R. Geraldes *et al.*, “Mechatronics Concepts for the New High-Dynamics DCM for Sirius”, in *Proc. MEDSI’16*, Barcelona, Spain, Sep. 2016, paper MOPE19, pp. 44-47, doi : 10.18429/JACoW-MEDSI2016-MOPE19
- [7] M. Saveri Silva *et al.*, “Thermal Management and Crystal Clamping Concepts for the New High-Dynamics DCM for Sirius”, in *Proc. MEDSI’16*, Barcelona, Spain, Sep. 2016, paper TUPE15, pp. 194-197, doi : 10.18429/JACoW-MEDSI2016-TUPE15
- [8] R. M. Caliori *et al.*, “System Identification and Control for the Sirius High-Dynamic DCM”, in *Proc. ICALEPCS’17*, Barcelona, Spain, Oct. 2017, paper TUSH203, pp. 997-1002, doi : 10.18429/JACoW-ICALEPCS2017-TUSH203
- [9] G.B.Z.L. Moreno *et al.*, “Rapid Control Prototyping Tool for the Sirius High-Dynamic DCM”, in *Proc. ICALEPCS’17*, Barcelona, Spain, Oct. 2017, paper THPHA214, pp. 1941-1946, doi : 10.18429/JACoW-ICALEPCS2017-THPHA214
- [10] R. R. Geraldes *et al.*, “Granite Benches for Sirius X-ray Optical Systems”, presented at MEDSI’18, Paris, France, June 2018, paper THPH12, this conference.
- [11] R. M. Caliori *et al.*, “Studies on Flow-Induced Vibrations for the New High-Dynamics DCM for Sirius”, in *Proc. MEDSI’16*, Barcelona, Spain, Sep. 2016, paper MOPE02, pp. 8-11, doi : 10.18429/JACoW-MEDSI2016-MOPE02